POPs to COFs by Post-modification: CO_2 Chemisorption and Dissolution

Ayham A. Aladwan,[a] Abdussalam K. Qaroush,*[a] Ala'a F. Eftaiha,[b] Suhad B. Hammad,[a] Feda M. Al-Qaisi,[b] Khaleel I. Assaf,[c] Timo Repo[d]

[a] Department of Chemistry, Faculty of Science, The University of Jordan, 11942 Amman, Jordan.
[b] Department of Chemistry, Faculty of Science, The Hashemite University, Zarqa 13133, Jordan.
[c] Department of Chemistry, Faculty of Science, Al-Balqa Applied University, Al-Salt 19117, Jordan.
[d] Department of Chemistry, University of Helsinki, A.I. Virtasen aukio 1, 00014 Helsinki, Finland.

Electronic Supplementary Information

Abbreviations

- POP-5; the methylene group serves as the spacer within the aromatic diamine (NH_2-C_6H_4-CH_2-C_6H_4-NH_2).
- O-POP (**6**); the oxygen atom serves as the spacer within the aromatic diamine (NH_2-C_6H_4-O-C_6H_4-NH_2).
- S-POP (**7**); the sulfur atom serves as the spacer within the aromatic diamine (NH_2-C_6H_4-S-C_6H_4-NH_2 based COF).
- SO_2-POP (**8**); the sulfone group serves as the spacer within the aromatic diamine (NH_2-C_6H_4-SO_2-C_6H_4-NH_2).
- Zn-COF: Zinc bromide-based COF (**9**).
- I-COF: Iminium-based COF (**10**).
- SA-COF: Secondary amine COF (**11**).
- A-COF: Ammonium-based COF (**12**).
- M-POP: Monoethanolamine-tethered POP (**13**).
- E-COF: Ethylenediamine-tethered COF (**14**).

Table of Contents

1. Synthesis of Porous Organic Polymers (POPs) and Covalent-Organic Frameworks (COFs)

1.1. Synthesis of Z-POP (5-8)

In a 100 mL round bottomed flask, the **Z**-substituted, aromatic diamine (**1-4**, 1.85 mmol, 3 eq.) and 1,3,5-Triformylbenzene (**TFB**, 200 mg, 1.23 mmol, 2 eq.) were mixed in 20 mL of anhydrous DMF at RT and transferred into a preheated sand bath at 140 °C for a period of time: (36 h for **5**; 52 h for **6**; 72 h for **7**; 96 h for **8**). The precipitate (**5**-**7**) was collected and washed with copious amounts of DMF, EtOH, and THF, respectively. In the case of **8** which showed complete solubility in DMF, it was suspended in a 150 mL DI H_2O, then the solid material centrifuged at 5000 rpm for 2 h; decanted and washed with copious amounts of EtOH and THF. The product was soaked in 50 mL THF for 4 days then dried in a vacuum oven (3 mbar) for 8 h at 60 °C.

(**5**, 0.50 g collected, yield by mass: 87.7%): **^{13}C CP-MAS NMR (500 MHz, ppm):** δ 44.4 (Ar-***C***H_2-Ar), (124.3, 133.3, 141.4, and 152.9 (Aromatic ring region)), 161.9 (R-***C***=N-R), 193.7 (Aldehyde functionality). **ATR-FTIR** (**400-4000 cm^{-1}**): 3018 υ(aryl C-H), 2860 υ(alkylene C-H), 1697 υ(C=O), 1623 υ(C=N), 1500 υ(C=C_{arom}). **TGA:** No weight loss up to 481 °C, the decomposition temperature at 80% weight loss (**T_{d80}**) took place at 516 °C. **PXRD**: **2θ:** 19.08°, 42.12°. **BET**: Surface area: 198.7 m^2.g^{-1}, Pore size: 3.48 nm, Average particle size: 301.9 Å.

(**6**, 0.37 g): **ATR-FTIR (400-4000 cm^{-1}):** 3031 υ(aryl C-H), 1697 υ(C=O), 1621 υ(C=N), 1488 υ(aryl C=C), 1230 $υ_{as}$(C-O-C), 1199 $υ_s$(C-O-C). **TGA**: No weight loss up to 486 °C, the decomposition temperature at 80% weight loss (**T_{d80}**) took place at 535 °C. **PXRD**: **2θ:** 18.6°. **BET:** Surface area: 205.1 m^2.g^{-1}, Pore size: 3.88 nm, Average particle size: 292.6 Å.

(**7**, 0.40 g): **ATR-FTIR (400-4000 cm^{-1}):** 3047 υ(aryl C-H), 1699 υ(C=O), 1618 υ(C=N), 1481 υ(aryl C=C), 592 υ(C-S-C). **TGA**: No weight loss up to 467°C, the decomposition temperature at 80% weight loss ($\mathbf{T}_{d80}$) took place at 520 °C. **PXRD: 2θ:** 19.1˚.

(**8**, 0.22 g): **ATR-FTIR (400-4000 cm^{-1}):** 3475 υ_{as}(1˚ N-H), 3361 υ_{s}(1˚ N-H), 3047 υ(aryl C-H), 1693 υ(C=O), 1627 υ(C=N), 1502 υ(C=C_{arom}), 1282 υ_{as}(S=O), 1095 υ_{s}(S=O). **TGA**: No weight loss up to 466°C, the decomposition temperature at 80% weight loss ($\mathbf{T}_{d80}$) took place at 491 °C. **PXRD: 2θ:** 20.1˚.

1.2. Synthesis of Zn-COF (9)

In a 100 mL round bottomed flask, POP-**5** (**5**, 0.10 g) and zinc bromide ($ZnBr_2$, 0.10 g, 0.4 mmol), were mixed together in 10 mL anhydrous DMF at RT and transferred into a preheated sand bath at 140 °C for 72 h. The product was collected and washed with copious amounts of DMF, EtOH, and THF, respectively. The product was dried in a vacuum oven (3 mbar) for 8 h at 60 °C (0.10 g). **^{13}C CP-MAS (500 MHz, ppm):** δ 42.9 (Ar-***C***H_2-Ar), (123.3, 131.8, 140.2, and 151.3 (Aromatic ring region), 160.5 (R-***C***=N-R), 193.9 (Aldehyde functionality). **ATR-FTIR (400-4000 cm^{-1}):** 3020 υ(aryl C-H), 2858 υ(alkylene C-H), 1697 υ(C=O), 1623 υ(C=N), 1498 υ(C=C), 503 υ(Zn-N). **TGA:** No weight loss up to 453 °C, the decomposition temperature at 80% weight loss ($\mathbf{T}_{d80}$) took place at 488 °C. **PXRD: 2θ:** 3.1˚, 19.4˚, 25.3˚, 32.6˚, 34.4˚, 36.4˚,38.8˚, 43.0˚, 46.8˚, 51.5˚, 53.8˚, 56.8˚.

1.3. Synthesis of I-COF (10)

In a 100 mL round bottomed flask, 1 mL of HBr.AcOH was slowly added at ice-cooled conditions to a suspension of POP-**5** (**5**, 0.10 g) in 70 mL ethyl acetate. The reaction left to stir overnight at RT. The product was collected and washed with copious amount of EtOAc, then dried in a vacuum

oven (3 mbar) for 8 h at 60 °C (0.15 g). **^{1}H NMR (500 MHz, DMSO-d_6, ppm):** δ 10.21, 10.20, 8.85, 8.69, 8.55, 7.40, 7.39, 7.36, 7.34, 7.31, 7.29, 7.27, 4.00, 3.70. **^{13}C NMR (125 MHz, DMSO-d_6, ppm):** δ 192.61, 170.84, 141.70, 137.82, 134.94, 134.30, 130.47, 130.09, 129.81, 123.96, 121.98, the spacer peak at *ca.* 40 ppm is overlapped with the DMSO-d_6 peak. **ATR-FTIR (400-4000 cm^{-1}):** 3432 υ(N^+-H), 3035 υ(aryl C-H), 2861 υ(alkylene C-H), 1697 υ(C=O), 1660 υ($C=N^+$), 1625 υ(C=N), 1498 υ(C=C). **TGA:** No weight loss up to 150 °C, the decomposition temperature at 80% weight loss ($\mathbf{T}_{d80}$) took place at 244 °C. **PXRD**: **2θ:** 7.4°, 9.4°, 14.8°, 20.1°, 21.9°, 22.6°, 23.6°, 25.6°, 26.1°, 27.1°, 29.1°, 32.6°. **BET**: Surface area: 43.4 $m^2.g^{-1}$, Pore size: 1.78 nm, Average particle size: 1383.1 Å.

1.4. Synthesis of SA-COF (11)

In a 50 mL round bottomed flask, POP-**5** (**5**, 50 mg) was suspended in 30 mL MeOH followed by the addition of $NaBH_4$ (1.00 g, 2.64 mmol) over 10 min, under ice-cooled conditions and reaction left to stir for 1 h. Then, left for an additional 18 h at RT. The product was collected and washed with copious amounts of MeOH, and THF, and dried in a vacuum oven (3 mbar) for 8 h at 60 °C (56 mg). **^{13}C CP-MAS (500 MHz, ppm):** δ 42.7 (Ar-***C***H_2-Ar), 66.9 (***C***-N-H), (123.3, 131.7, 140.1, and 151.3 (Aromatic ring region), 160.9 (R-***C***=N-R), 191.5 (Aldehyde functionality). **ATR-FTIR (400-4000 cm^{-1}):** 3417 υ(O-H) and υ(N-H), 3093 υ(aryl C-H), 2854 υ(alkylene C-H), 1625 υ(C=N), 1610 υ(C-N-H), 1512 υ(N-H), 1477 υ(C=C), 1340 υ(C-N). **TGA:** No weight loss up to 457 °C, the decomposition temperature at 80% weight loss ($\mathbf{T}_{d80}$) took place at 483 °C. **PXRD: 2θ:** 6.8˚, 8.5˚, 10.3˚, 11.1˚, 13.5˚, 15.0˚, 25.1˚, 27.1˚, 29.1˚, 30.4˚, 33.4˚, 34.9˚, 38.6˚, 40.1˚, 41.4˚. **BET:** Surface area: 18.1 $m^2.g^{-1}$, Pore size: 2.73 nm, Average particle size: 3309.5 Å.

1.5. Synthesis of A-COF (12)

In a 100 mL round bottomed flask, 1 mL of HBr.AcOH was slowly added at ice-cooled conditions to a suspension of SA-COF (**11**, 0.10 g) in 70 mL EtOAc. The reaction left to stir at RT overnight. The product was collected and washed with copious amount of EtOAc and dried in a vacuum oven (3 mbar) for 8 h at 60 °C (0.13 g). **^{1}H NMR (500 MHz, DMSO-d_6, ppm):** δ 10.21, 10.20, 10.09, 8.89, 8.88, 8.77, 8.71, 8.69, 8.61, 8.57, 8.54, 8.46, 8.39, 8.32, 8.26, 8.15, 8.11, 7.90, 7.50, 7.33, 7.29, 7.16, 7.01, 4.60, 4.00, 3.88, 3.76. **^{13}C NMR (125 MHz, DMSO-d_6, ppm):** δ 192.64, 166.76, 158.91, 141.66, 137.82, 134.95, 134.29, 130.45, 130.08, 129.81, 123.96, 123.82, 121.99, 60.24, 40.39. **ATR-FTIR (400-4000 cm^{-1}):** 3380 υ(N^+-H), 3031 υ(aryl C-H), 2833 υ(alkylene C-H), 1693 υ(C=O), 1658 υ(C=N^+), 1627 υ(C=N), 1569 υ(C-N^+-H), 1506 υ(aryl C=C), 1430 υ(N^+-H). **TGA:** No weight loss up to 157 °C, the decomposition temperature at 80% weight loss ($\mathbf{T}_{d80}$) took place at 260 °C. **PXRD**: **2θ:** 22.1°, 26.0°, 30.2°, 43.1°, 50.9°, 53.3°.

1.6. Synthesis of M-POP (13)

In a 100 mL round-bottomed flask, POP-**5** (**5**, 500 mg) was suspended into a freshly distilled monoethanolamine (**MEA**, 50 mL) under N_2 at RT, and transferred into a preheated sand bath at 100 °C for 72 h. The reaction was cooled to RT and the post-modified product was collected and washed with copious amounts of Et_2O, and ACN, respectively. The product was soaked in 50 mL ACN for 1 day, then dried in vacuum oven (3 mbar) for 8 h at 60 °C (450 mg collected). **ATR-FTIR (400-4000 cm^{-1}):** 3351 υ(O-H), 3022 υ(aryl C-H), 2869 υ(aliphatic C-H), 1697 υ(C=O), 1619 υ(C=N), 1598 and 1502 υ(aryl C=C). **TGA:** No weight loss up to 446 °C, the decomposition temperature at 80% weight loss ($\mathbf{T}_{d80}$) took place at 476 °C. **PXRD: 2θ:** 18.3˚, 23.5˚, 30.2˚, 43.0˚.

1.7. Synthesis of E-COF (14)

In a 100 mL round-bottomed flask, POP-**5** (500 mg) together with a freshly distilled ethylenediamine (**EDA**, 50 mL), mixed under N_2 at RT and transferred into a preheated sand bath at 100 °C for 72 h. The precipitate formed after cooling the reaction in the freezer for 30 min (-20 °C), collected and washed with copious amounts of Et_2O, and ACN, respectively. The product was soaked in 50 mL ACN for 1 day then dried in vacuum oven (3 mbar) for 8 hours at 60 °C (400 mg collected). **ATR-FTIR (400-4000 cm^{-1}):** 3153 υ(N-H carbamate), 3049 υ(aryl C-H), 2950 υ(NH_3^+), 2826 υ(aliphatic C-H), 1768 υ(R-NH-COO amide I band), 1672 υ(R-NH-CO_2^- NH_3^+-R), 1641 υ(C=N), 1583 and 1496 υ(aryl C=C), 1550 υ(R-NH-COO amide II band), 1139 υ(in-plane aryl C-H), 644 υ(out-of-plane aryl C-H). **TGA:** No weight loss up to 142 °C, the decomposition temperature at 80% weight loss ($\mathbf{T}_{d80}$) took place at 157 °C. **PXRD: 2θ:** 11.2˚, 18.6˚, 20.6˚, 22.3˚, 23.0˚, 24.7˚, 27.8˚, 32.0˚, 35.3˚, 36.1˚, 39.6˚, 50.3˚, 51.4˚, 56.9˚.

1.8. Dissolution Protocol of M-POP/DBU Binary System

In a sealed 12 mL glass vial coupled with magnetic stirrer, 10 mg of M-POP was added under a constant flow of N_2 followed by the addition of 0.5 mL **DBU** at RT. The suspension reaction left to stir for 48 h under atmospheric CO_2/H_2O conditions.

2. Characterization of nano materials

2.1. Z-POPs (Z: O, S, SO_2)

ATR-FTIR analysis was performed to further prove the synthesis of our materials. Herein, we report the co-condensation of **6-8** (**Figure S1**) by the formation of C=N stretching band at *ca.* 1623 cm^{-1} which clearly confirm the formation of imine bond.[1] The signal at *ca.* 1697 cm^{-1} represents stretching band of C=O for the aldehyde moiety within the network of imine POPs which has been observed in another literature published when the material have been synthesized using DMF.[2] Further, disappearance of 3421 cm^{-1} and 3405 cm^{-1} bands in **1** which corresponds to asymmetric and symmetric stretching vibrations of primary amine respectively (**Figure S1**), except for **8** which exhibited the presence of primary amine end group asymmetric and symmetric stretching bands at 3475 cm^{-1} and 3361 cm^{-1}, respectively. That might be attributed to the reversibility of the reaction due to high electron withdrawing effect of the sulfone group which has weakened the nucleophilicity of the amine group. For the aromatic C=C vibrations, it was observed at *ca.* 1500 cm^{-1}, aryl C-H and alkylene C-H vibrations were obtained at *ca.* 3018 cm^{-1} and 2860 cm^{-1} respectively. The TGA profile (**Figure S2**) for **6** started to decompose at 486 °C together with **7** and **8** at 467 °C and 466 °C, respectively. While the T_{d80} 535 °C, 520 °C, and 466 °C for **6-8**, respectively. The materials exhibited high thermal stability due to rigidity of the structures where the results indicated the nature of polymeric materials. The PXRD results for (**6-8**, **Figure S3**) suggests an amorphous nature of the synthesized imines due to inherent stacking disorder that affects crystallinity pattern.[3]

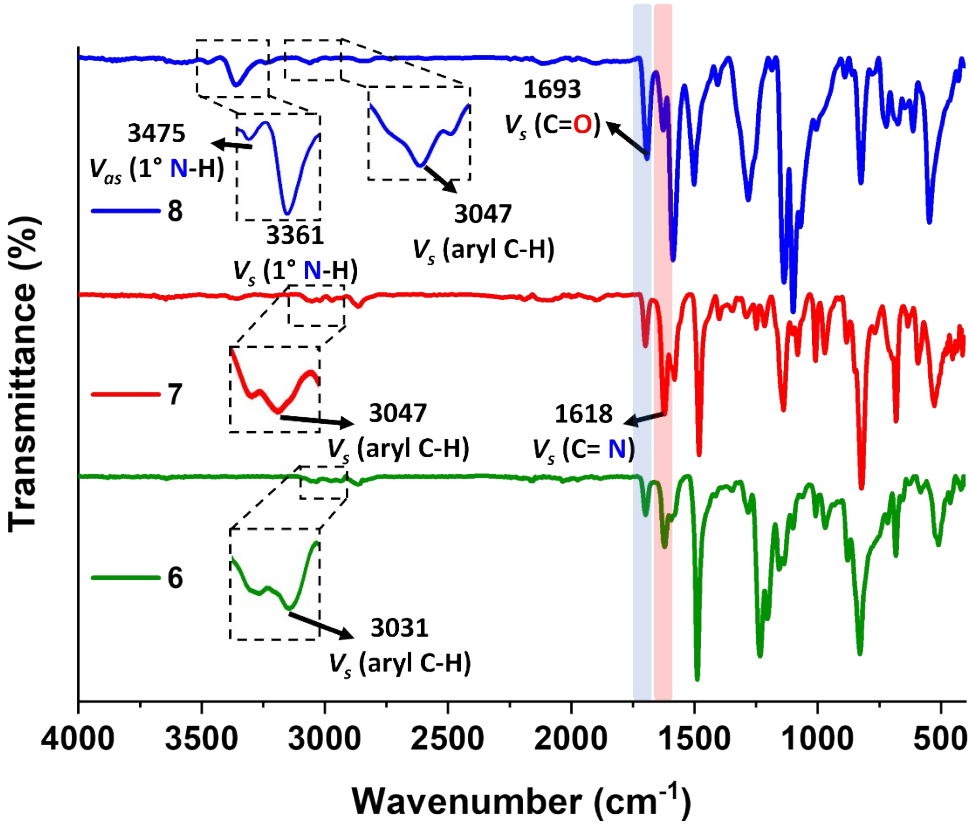

Figure S1. ATR-FTIR spectra of **6-8**; (O-POP, green), (S-POP, red), and (SO_2-POP, blue).

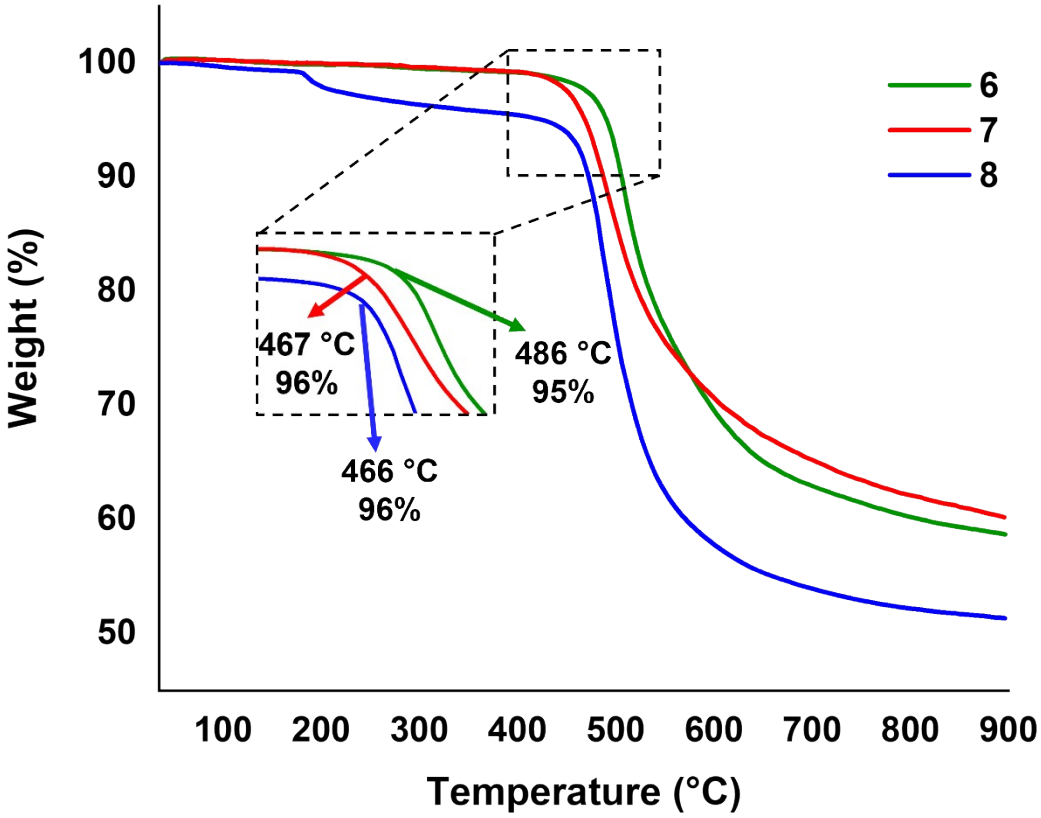

Figure S2. TGA analyses of **6-8**; (O-POP, green), (S-POP, red), and (SO_2-POP, blue).

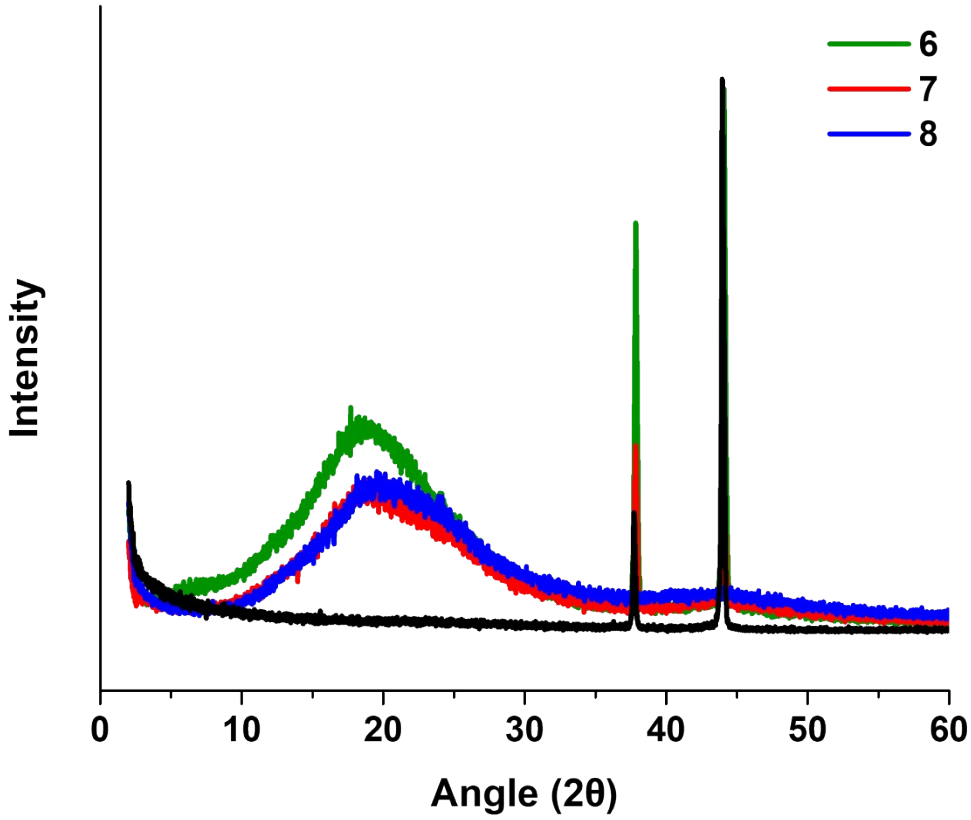

Figure S3. PXRD analyses of **6-8**; (O-POP, green), (S-POP, red), (SO_2-POP, blue), (Aluminum sample holder, black).

2.2. POP-5s (Zn, I, SA, A)

The following chemical transformations: **I.** Reduction, **II.** Coordination with zinc metal, and **III.** Quaternarization reactions were performed to enhance the performance of POP-5s for the purpose of CO_2 capture and utilization. These modifications were chosen for the commercial availability and cost-effectiveness of **1**, which serves as a precursor of compound **5**.

I. <u>Imine reduction:</u> Sodium borohydride was used as a reducing agent for the production of a secondary amine COF (**SA**-COF, **11**), in which the chemical shift of the methylene carbon (***C***H_2-NH) appeared at 66.9 ppm, alongside the imine carbon centered at 160.9 ppm as indicated by CP-

MAS (**Figure S4**), this fortified a partial reduction process.[4] Moreover, as shown in the ATR-FTIR spectrum, a shoulder appeared at 1610 cm^{-1} together with an intense peak centered at 1340 cm^{-1} associated with the bending mode of (CN-H), along with the stretching mode of (C-N-C),[5] respectively, (**Figure S5**). Also, the low chemoselectivity of $NaBH_4$ resulted in the transformation of the aldehyde contained within the network into a primary alcohol as a broadened band was observed as a result of the stretching mode of both functional groups (O-H and N-H) coupled peaks positioned at 3417 cm^{-1}. The thermal stability exhibited an initial decomposition temperature of 457 °C (with a T_{d80} value of 483 °C) as compared to **5** which started at 481 °C. It is noteworthy that PXRD demonstrated enhanced crystallinity due to the introduction of H-bonding along with the π-π stacking.

II. Coordination with Zinc metal: Successful coordination of **5** with $ZnBr_2$ was performed under anhydrous conditions, which resulted in a macro-layered zinc complex (**Zn**-COF, **9**) as indicated by a new Zn-N band at 503 cm^{-1}.[6] TGA trace showed an initial decomposition that started at 453 °C, (less thermal stability than **5**), which might be attributed to the weakly-coordinated metal dative bond (Zn-N). The PXRD revealed better crystallinity behavior, where this change is referred to the insertion of the metallic nuclei. As revealed by the Atomic Absorption Spectroscopy (AAS) measurements, the percentage of Zn was 31.7% (by mass) (**Figure S6**).

III. Quaternarization of imines/amines: Reaction of either **5** or **11** with hydrobromic acid obtained the iminium COF (**I**-COF, **10**) and the ammonium-based COF (**A**-COF, **12**), respectively. ^{13}C NMR analysis in DMSO-d_6 indicated the quaternarization by the appearance of a peak at *ca.* 170.8 and 60.2 for imine and amine carbon respectively. This was further confirmed by the ATR-FTIR spectroscopy of **I**-COF, in which formation of iminium moiety $C=N^+$ stretching band at 1660 cm^{-1} and N^+-H vibrations observed at 3432 cm^{-1}. Nevertheless, the neutral imine presence at 1625

cm^{-1} indicated a partial quaternarization. **A**-COF was configured by the clear shift of CN^{+}-H band of **11** at 1610 to 1569 cm^{-1}. Further, a shift observed from 1512 cm^{-1} for the secondary amine N-H bending mode to 1430 cm^{-1}. Moreover, C=N^{+} vibrations are observed at 1658 cm^{-1} as a result of the aforementioned partial reduction process. The presence of N^{+}-H stretching vibrations at 3380 cm^{-1} further proved the quaternarization of **11**. TGA traces of **10** and **12** were examined in which a prominent decrease in the stability was observed with initial decomposition temperatures recorded at 150 and 157 °C, respectively. In addition, T_{d80} for **10** and **12** was 244 °C and 260 °C respectively. This might be attributed to Hofmann degradation pathways.[7] Also, PXRD for **10** and **12** showed a good crystallinity upon the appearance of sharper peaks as a result of the strong intermolecular forces introduced *viz.,* ionic bonding together with interlayer interactions that enhanced stacking of the imine-derived COFs.[8]

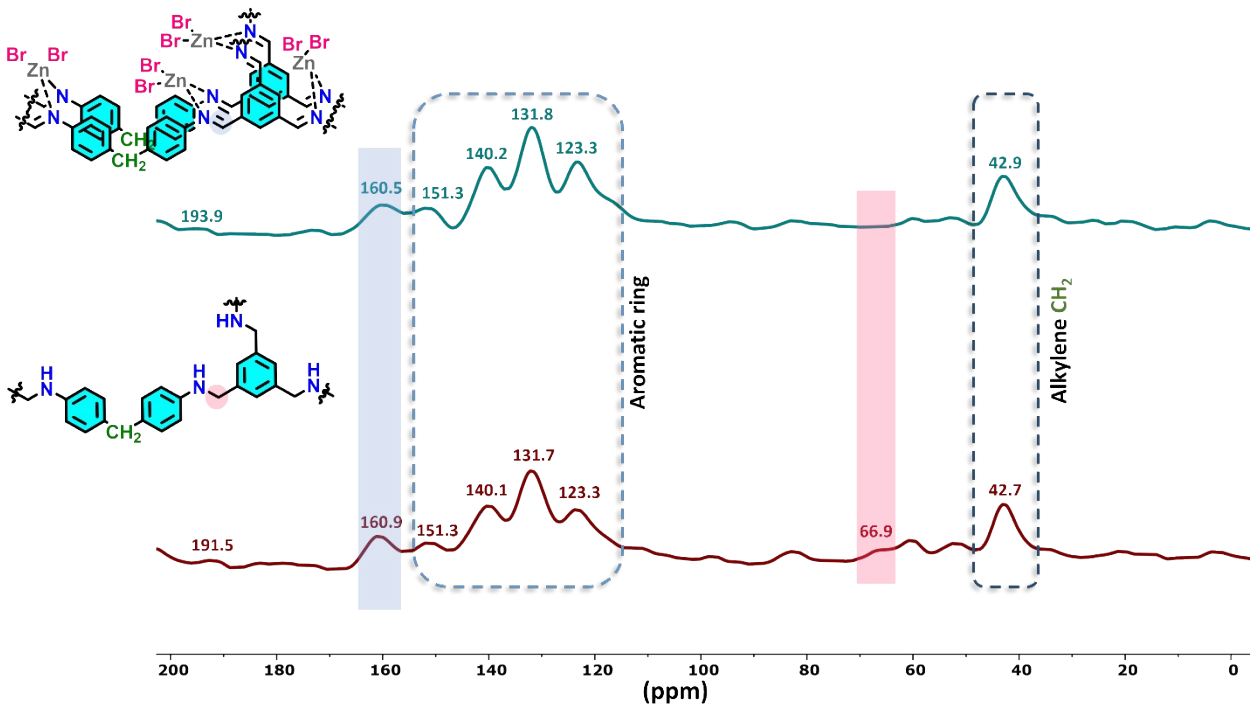

Figure S4. CP-MAS analyses for **9** (blue) and **11** (maroon).

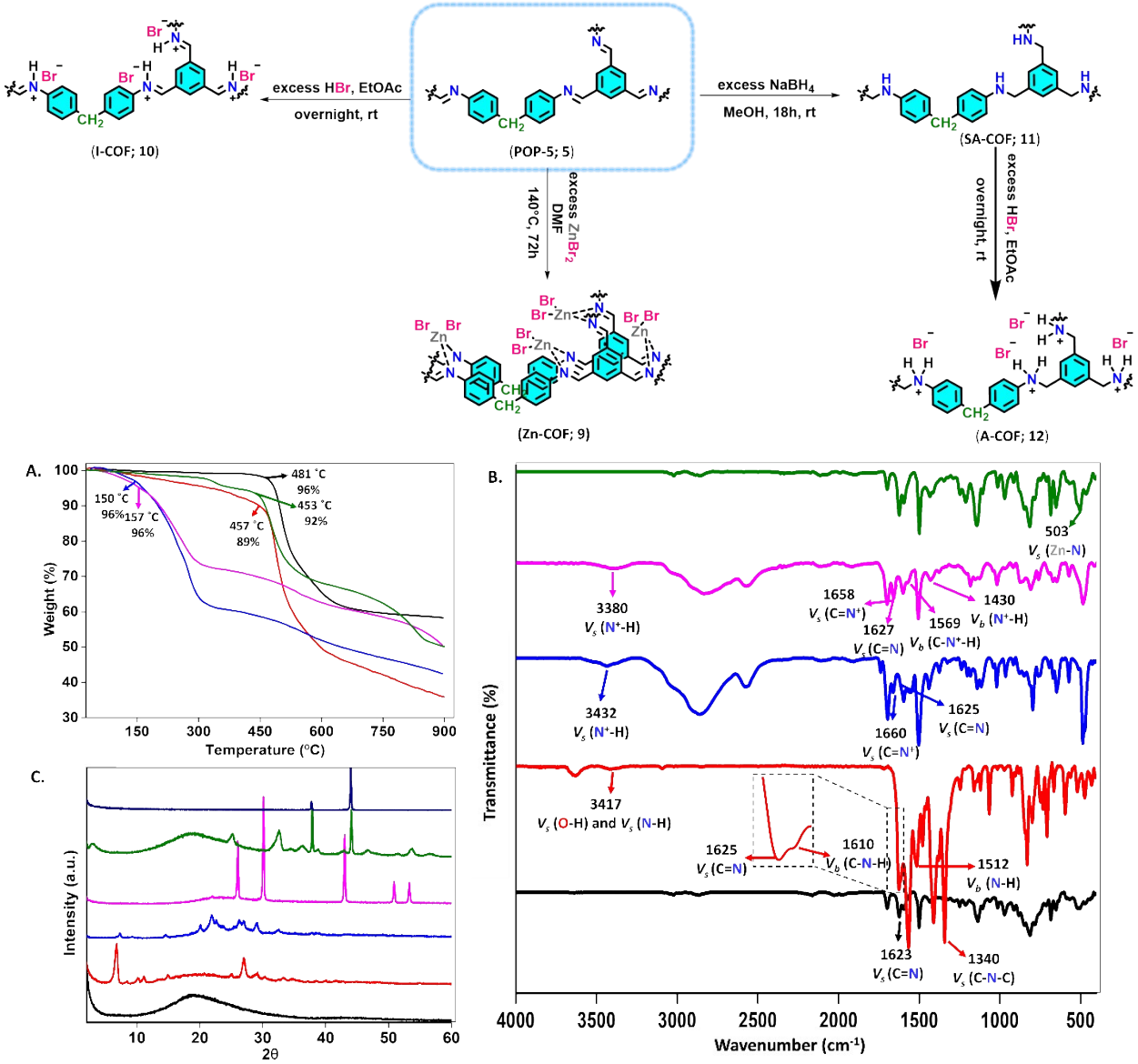

Figure S5. Schematic illustration of post-modified COFs synthesis. (**A-C**) TGA, ATR-FTIR, and PXRD analyses for POP-**5** (**5**, black), **Zn**-COF (**9**, green), **I**-COF (**10**, blue), **SA**-COF (**11**, red), **A**-COF (**12**, pink), and aluminum sample holder (**C**. dark blue).

2.3. AAS, BET, and DFT Analyses

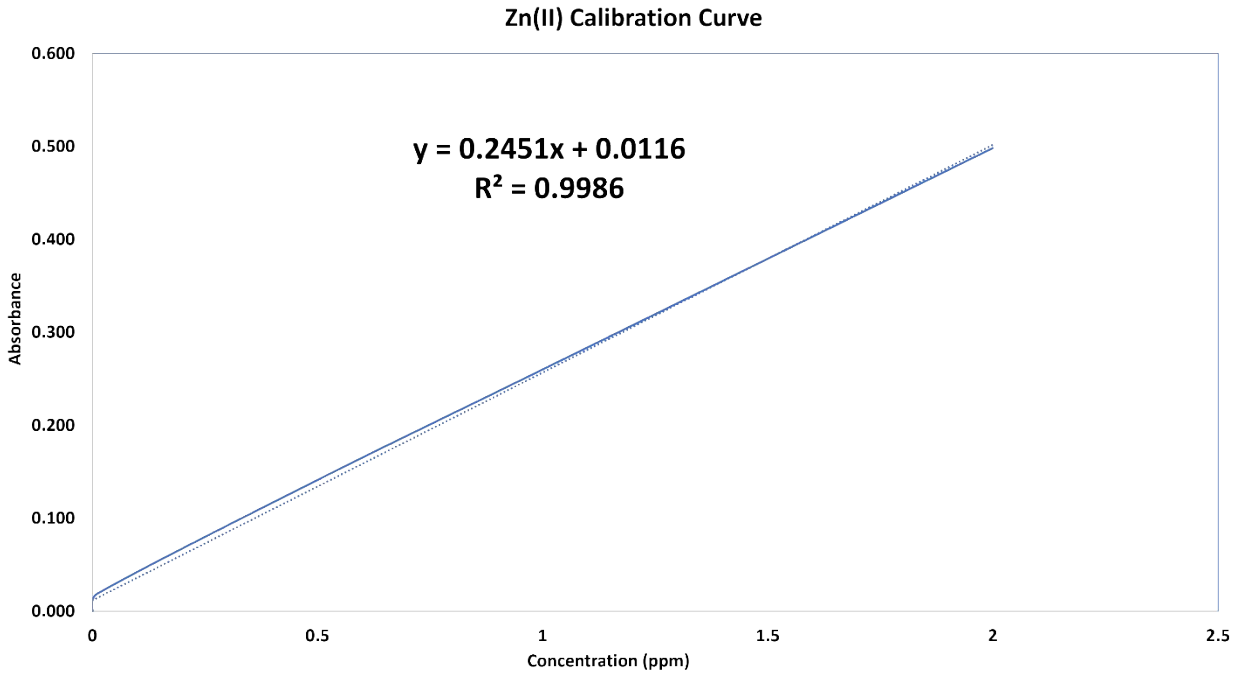

Figure S6. AAS calibration curve for the determination of zinc(II) content in **9**.

2.3.1. Conductivity and pH Sample Preparation Protocol

The aqueous solution of **E-COF** (500 ppm) was prepared and used to measure the conductivity of **14**, **E-COF/N_2** (bubbled with N_2 for 1 h at RT), and **E-COF/CO_2** (bubbled with CO_2 for 1 h at RT). Also, two separate blank experiments were prepared; (**EDA-carbamate**) 500 ppm aqueous solution of EDA, and (**DIW+CO_2)** 50 mL of DIW (both were bubbled with CO_2 for 1 h at RT before measuring the conductivity). The conductance of DI water was taken into consideration upon measuring the conductivity for all samples.

2.3.2. Atomic Absorption Spectroscopy

The calibration curve points were prepared following the following recipe: A stock solution of 1000 ppm $ZnBr_2$ prepared by the addition of 0.1 g $ZnBr_2$ in a 100 mL volumetric flask using 1% HCl as solvent. From the stock solution of $ZnBr_2$, starting from 0.01, 0.50, 1.00 to 2.00 ppm, a

calibration curve was made. Herein, samples were prepared by weighing 25 mg of **9** in 100 mL volumetric flask, digested using 5 mL of 33% HCl and filled up to volume using DI water.

2.3.3. BET Analysis

Table S1. The Brunauer-Emmett-Teller measurements of the synthesized COFs (**5**, **6**, **10-14**).

Material	S_{BET} ($m^2.g^{-1}$)	Pore Size (nm)	Average Particle Size (Å)
5	198.7	3.48	301.9
6	205.1	3.88	292.6
10	43.4	1.78	1383.1
11	18.1	2.73	3309.5
13	non-porous	N/A	N/A
14	55.4	N/A	N/A

2.3.4. DFT Calculations

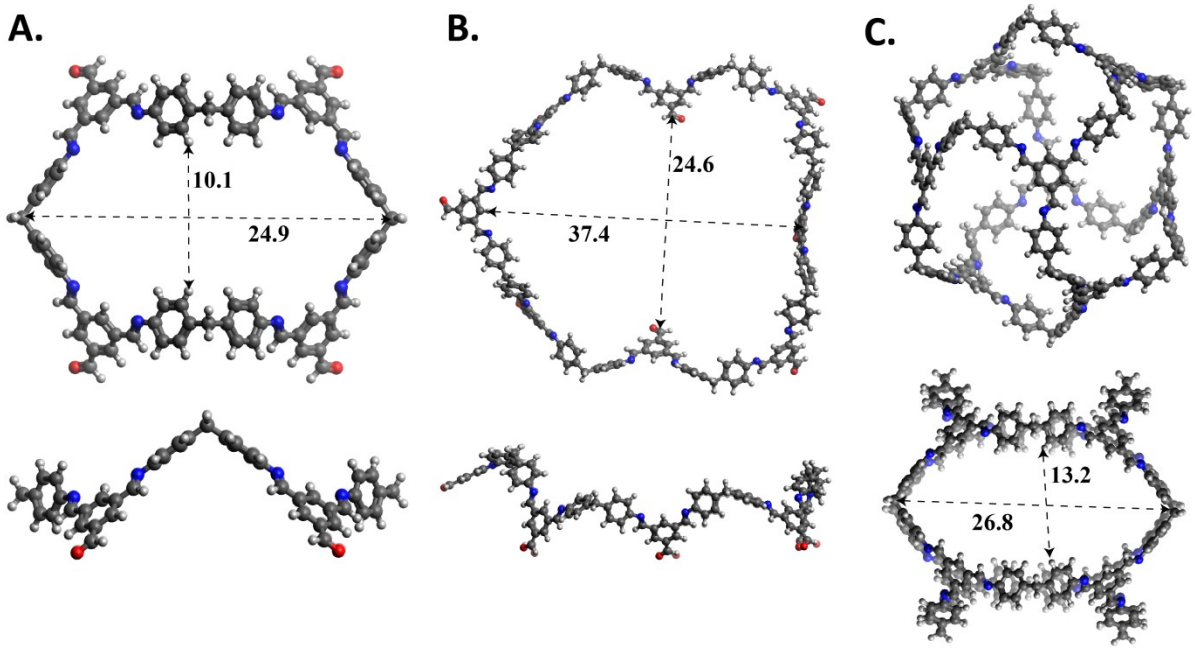

Figure S7. Postulated assembly structures based on DFT-calculations (B3LYP-D3/6-31+G*, in gas phase): **A.** and **B.** 2D-sheets and **C.** 3D-capsule. Distances are given in Angstrom.

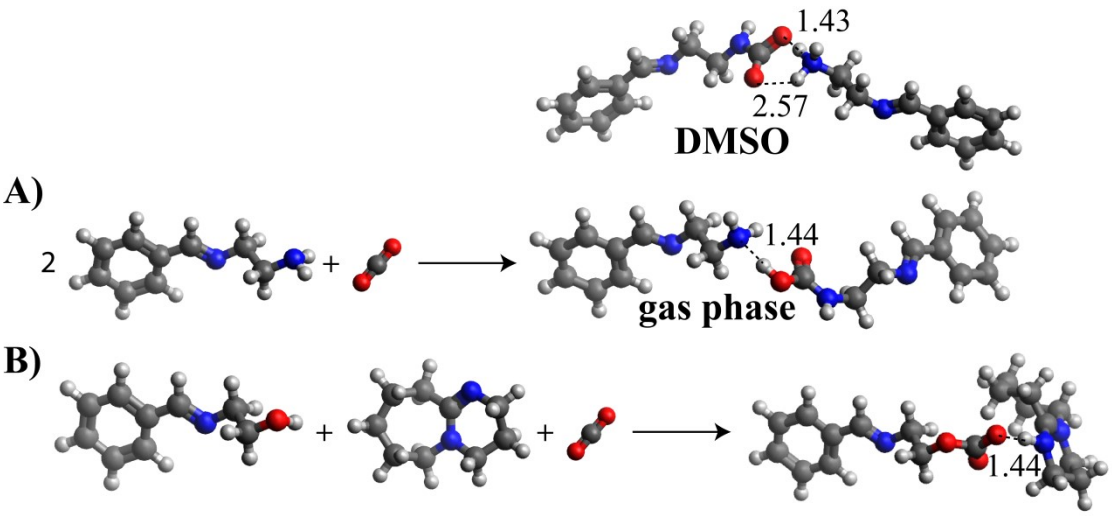

Figure S8. CO_2-capture reactions calculated at B3LYP-D3/6-311++G**: **A.** COF-terminated amine and **B.** POP-terminated alcohol. Distances are given in Angstrom.

3. CO_2 Adsorption Isotherms

Table S2. CO_2 sorption capacity (mmol CO_2/g sorbent) at 273 and 293 K.

Material	**Sorption Capacity**	
	273 K	**298 K**
POP-5	0.331	0.171
O-POP (6)	0.334	0.167
S-POP (7)	0.286	0.138
SO_2-POP (8)	0.192	0.131
Zn-COF (9)	0.317	0.114
SA-COF (11)	0.207	0.026
M-POP (13)	0.405	0.120
E-COF (14)	0.021	N/A

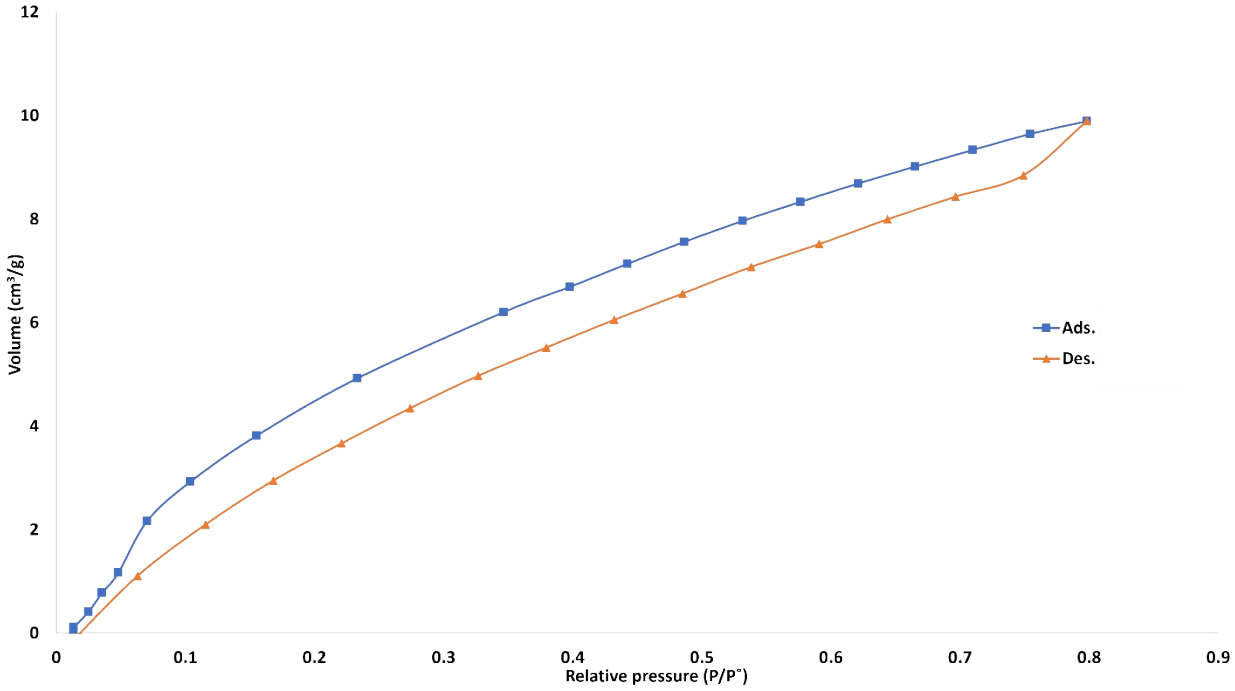

Figure S9. CO_2 adsorption (square)/desorption (triangle) isotherm of **5** at 273 K.

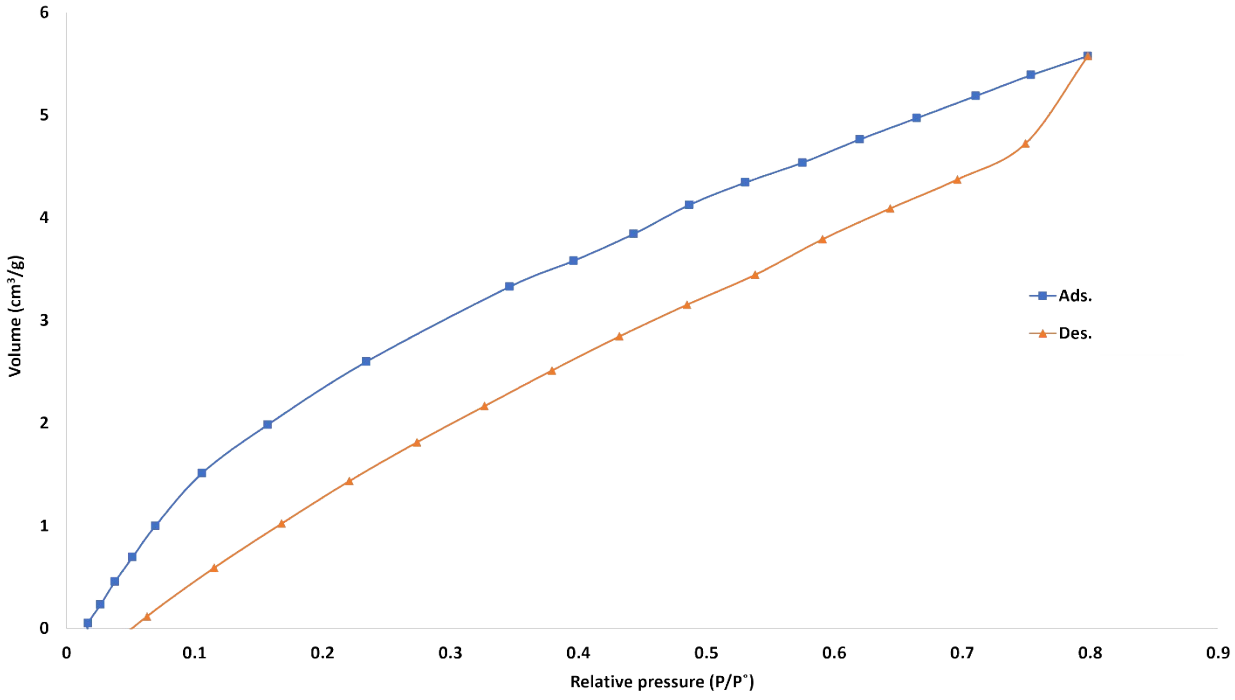

Figure S10. CO_2 adsorption (square)/desorption (triangle) isotherm of **5** at 298 K.

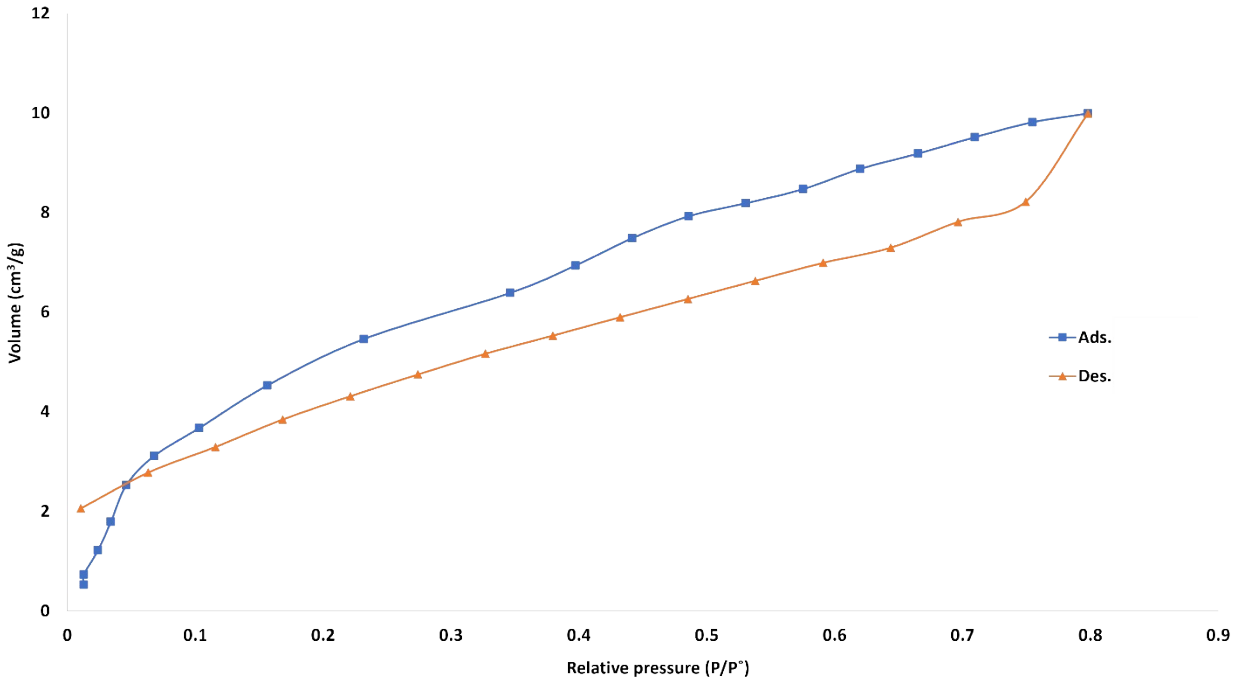

Figure S11. CO_2 adsorption (square)/desorption (triangle) isotherm of **6** at 273 K.

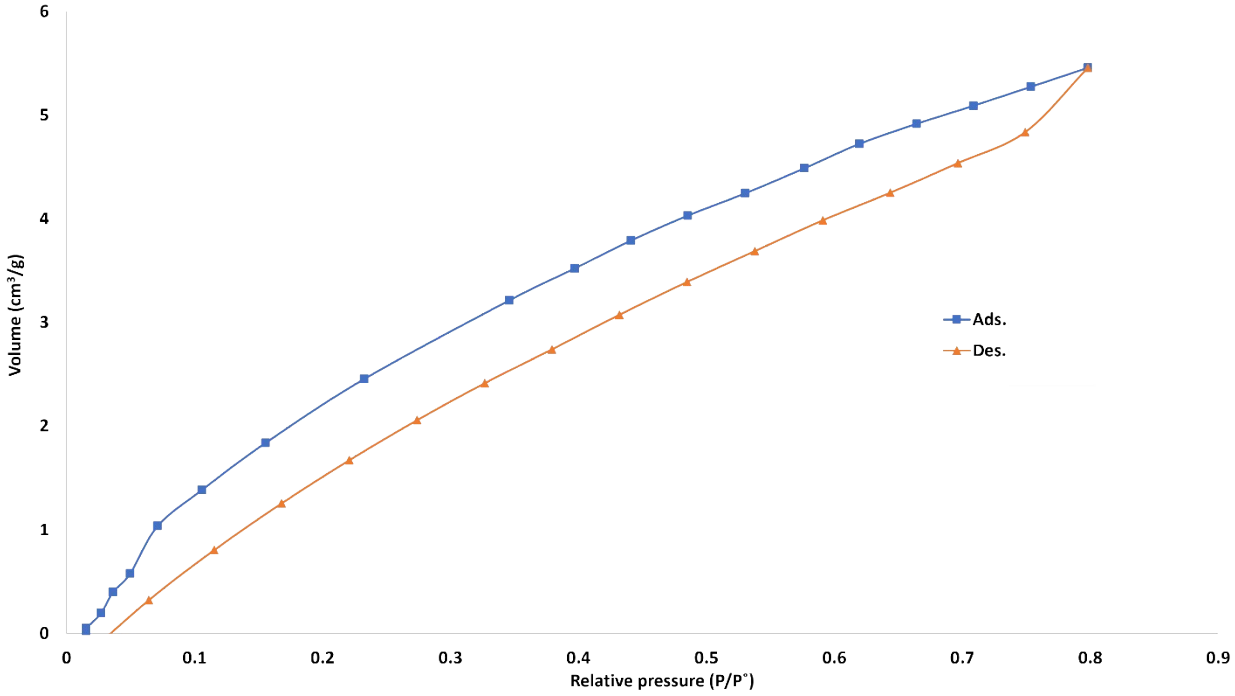

Figure S12. CO_2 adsorption (square)/desorption (triangle) isotherm of **6** at 298 K.

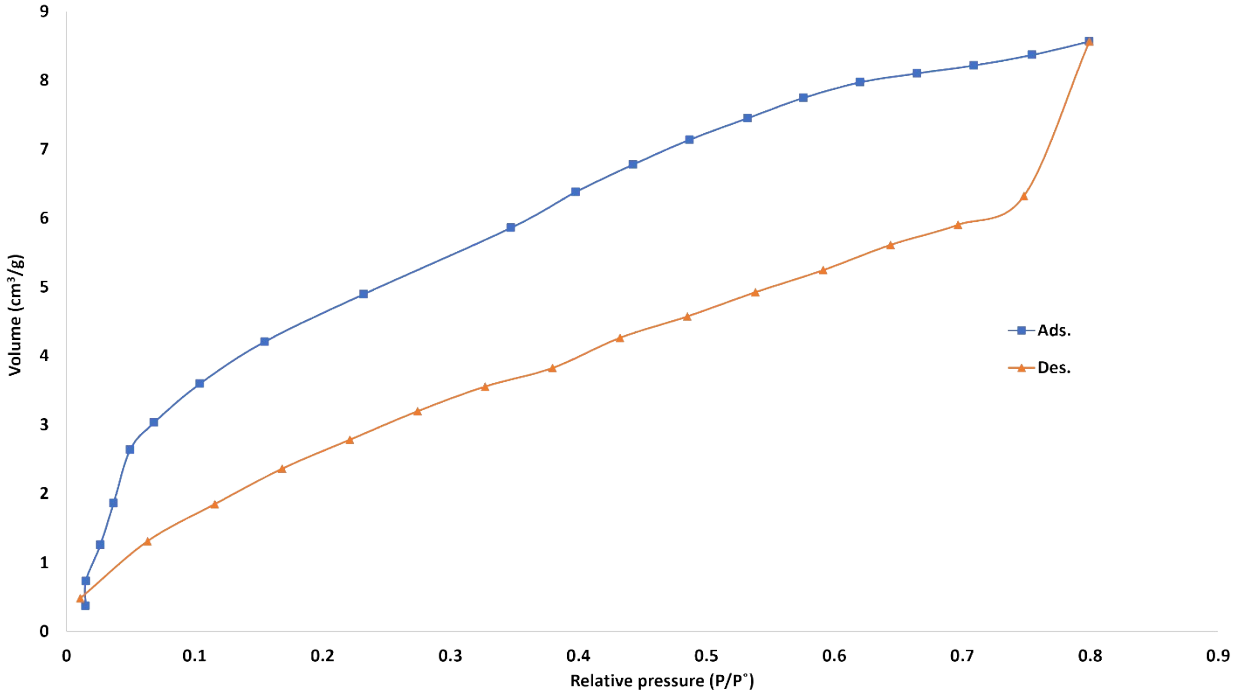

Figure S13. CO_2 adsorption (square)/desorption (triangle) isotherm of **7** at 273 K.

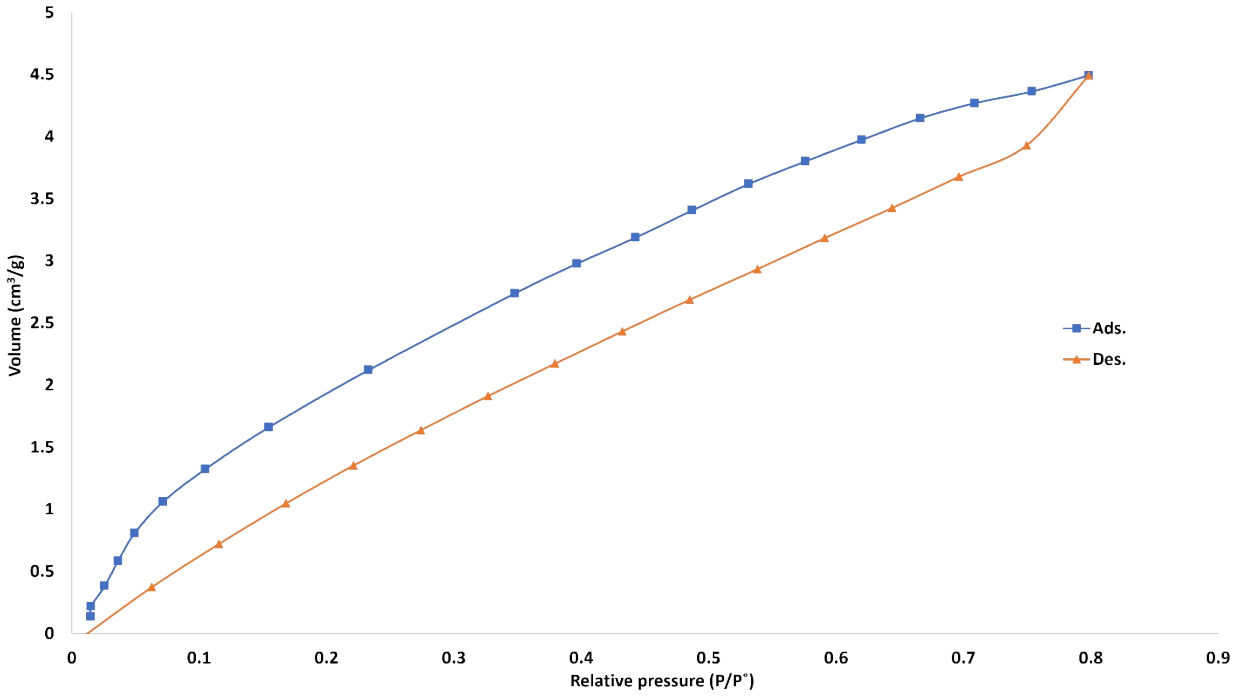

Figure S14. CO_2 adsorption (square)/desorption (triangle) isotherm of **7** at 298 K.

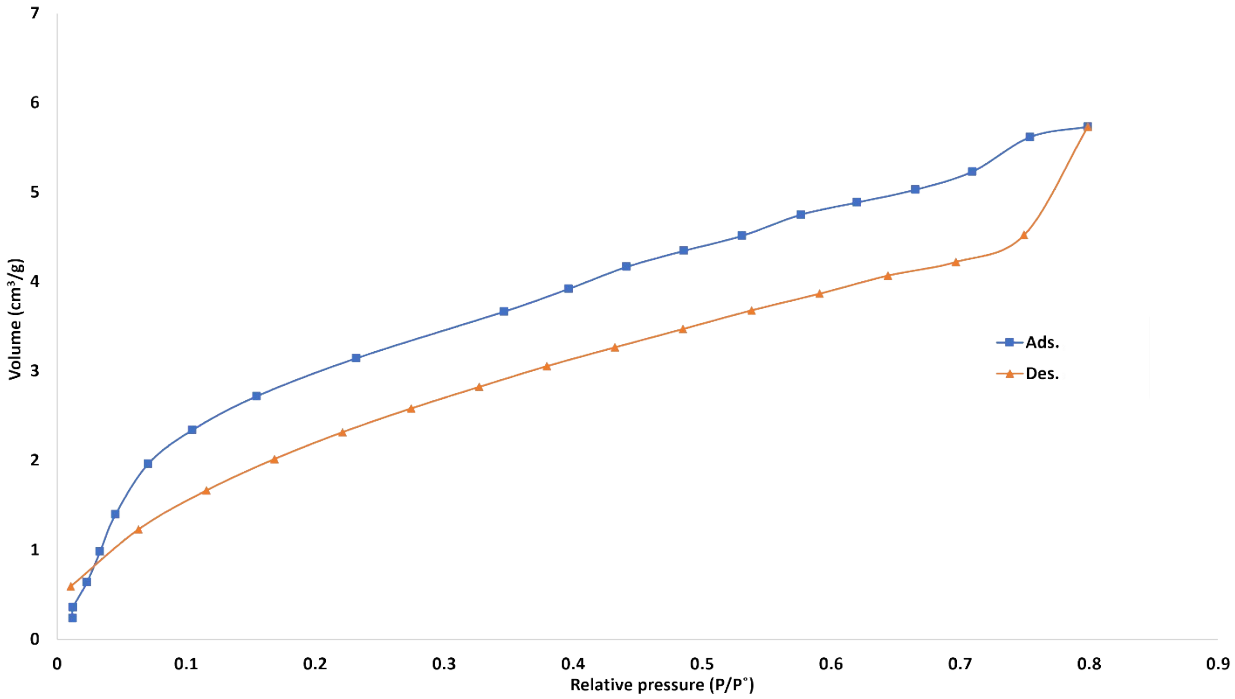

Figure S15. CO_2 adsorption (square)/desorption (triangle) isotherm of **8** at 273 K.

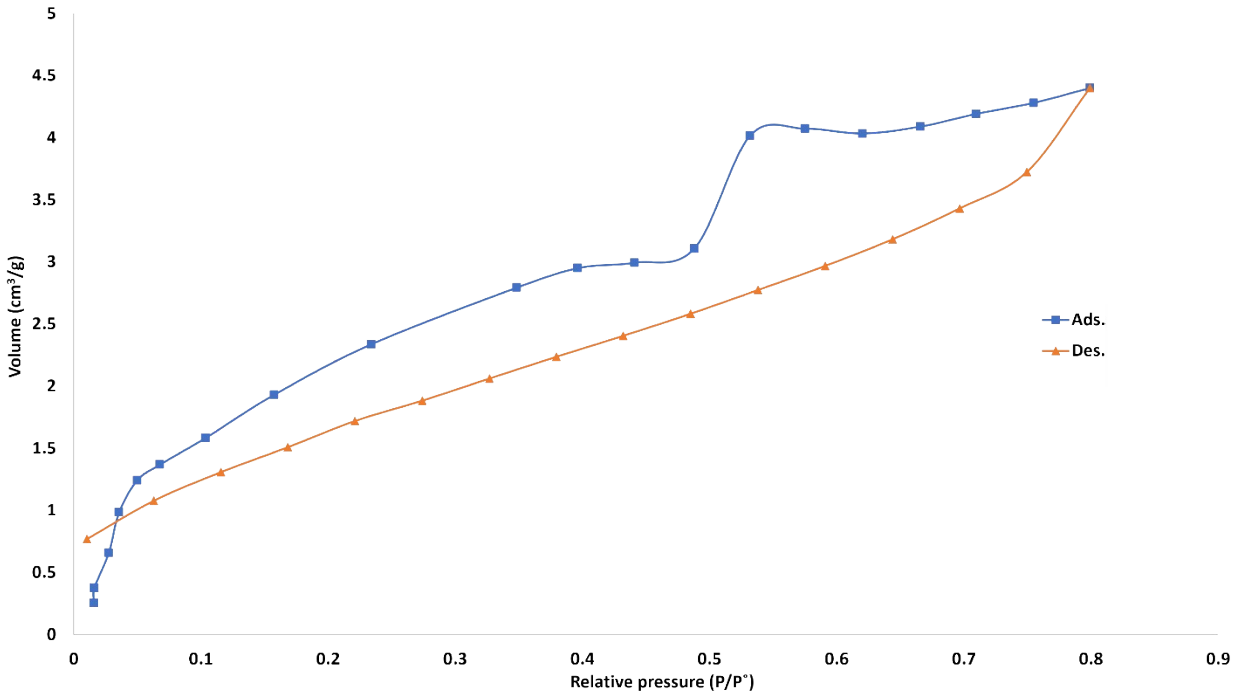

Figure S16. CO_2 adsorption (square)/desorption (triangle) isotherm of **8** at 298 K.

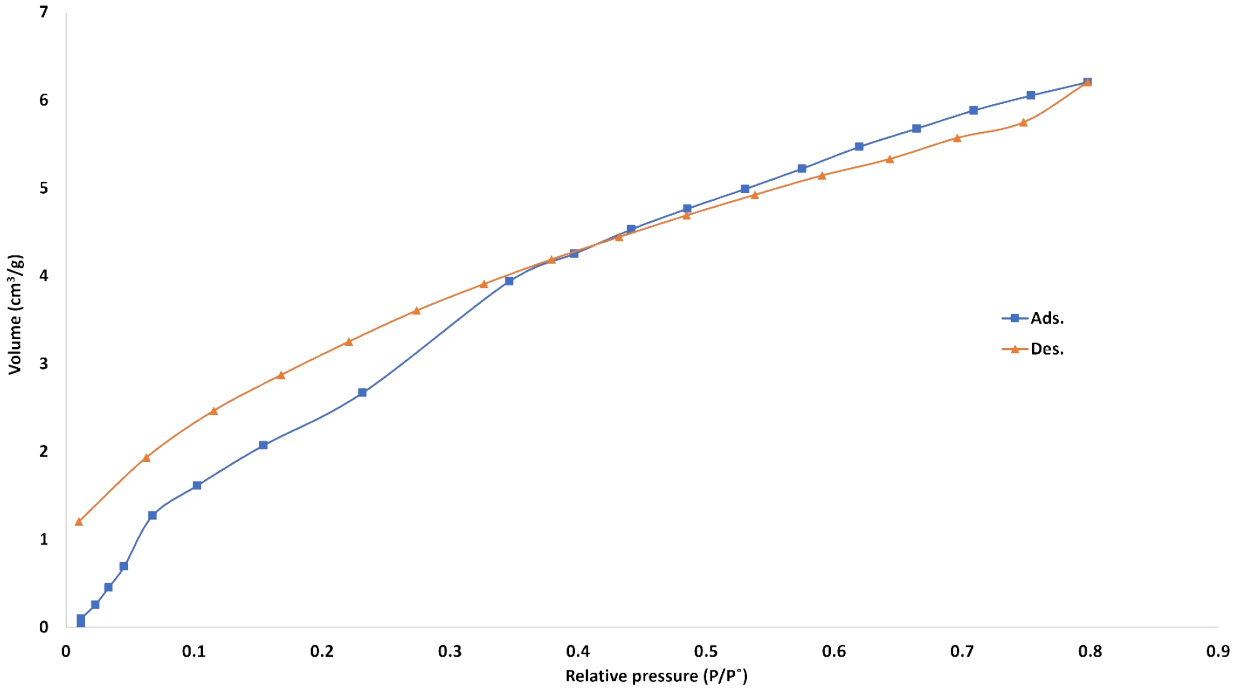

Figure S17. CO_2 adsorption (square)/desorption (triangle) isotherm of **11** at 273 K.

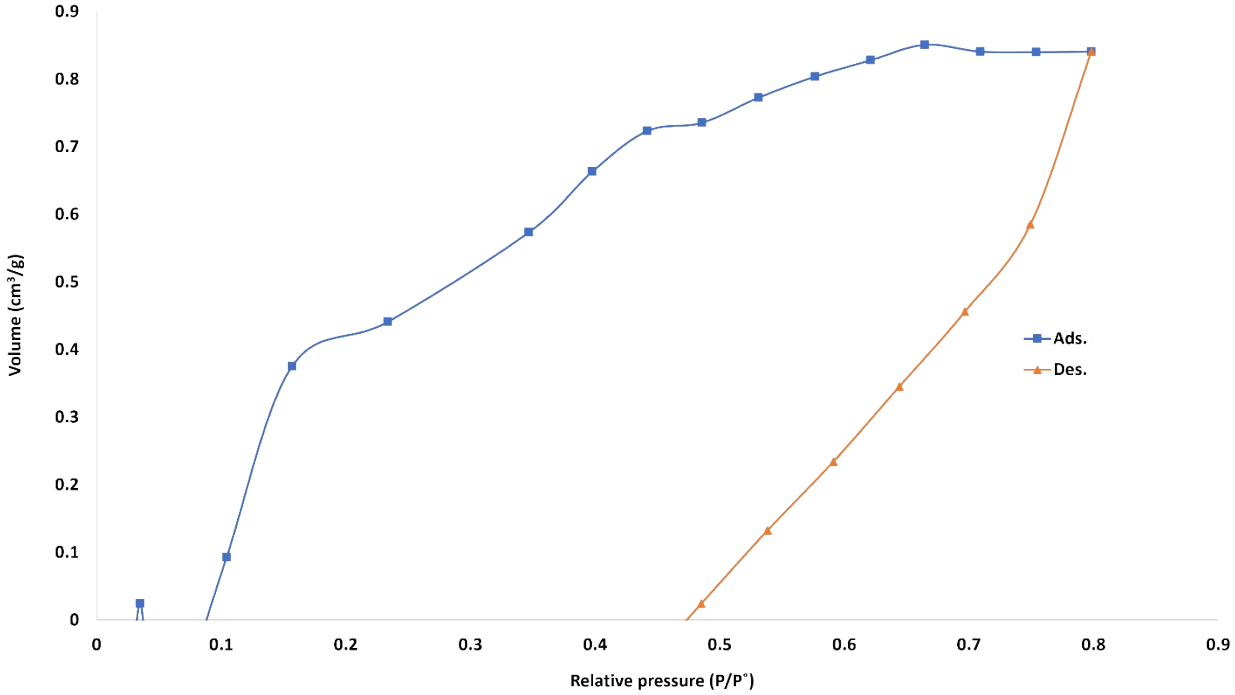

Figure S18. CO_2 adsorption (square)/desorption (triangle) isotherm of **11** at 298 K.

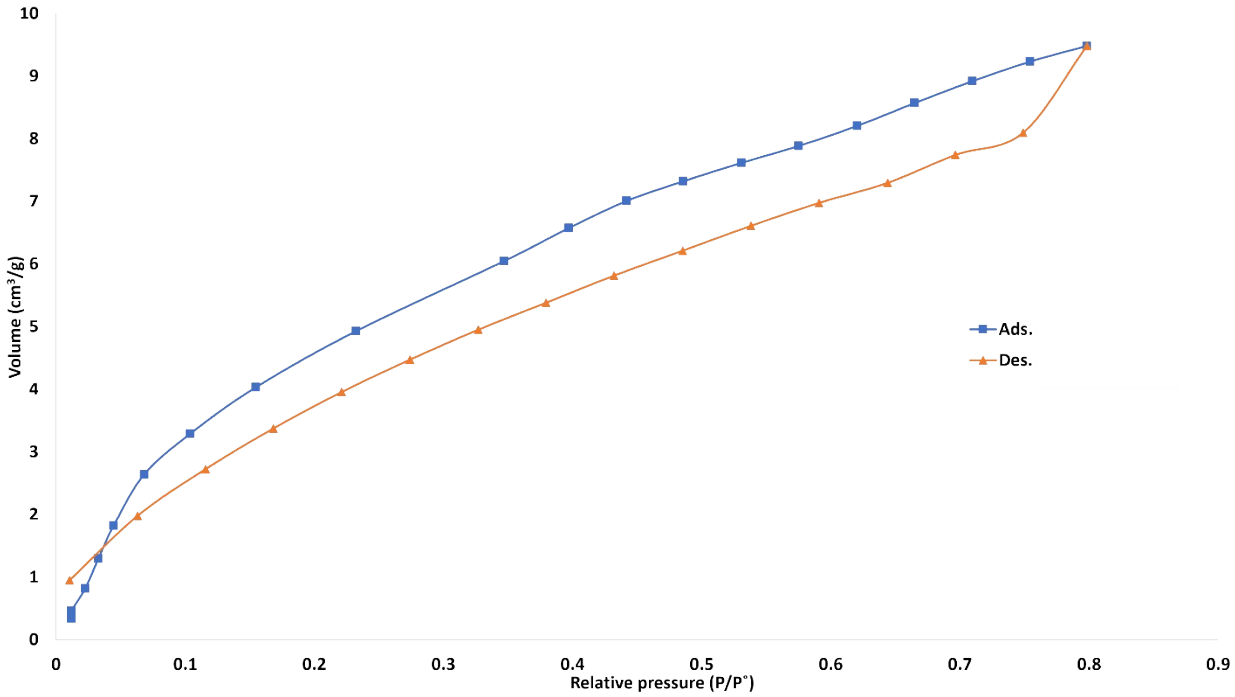

Figure S19. CO_2 adsorption (square)/desorption (triangle) isotherm of **9** at 273 K.

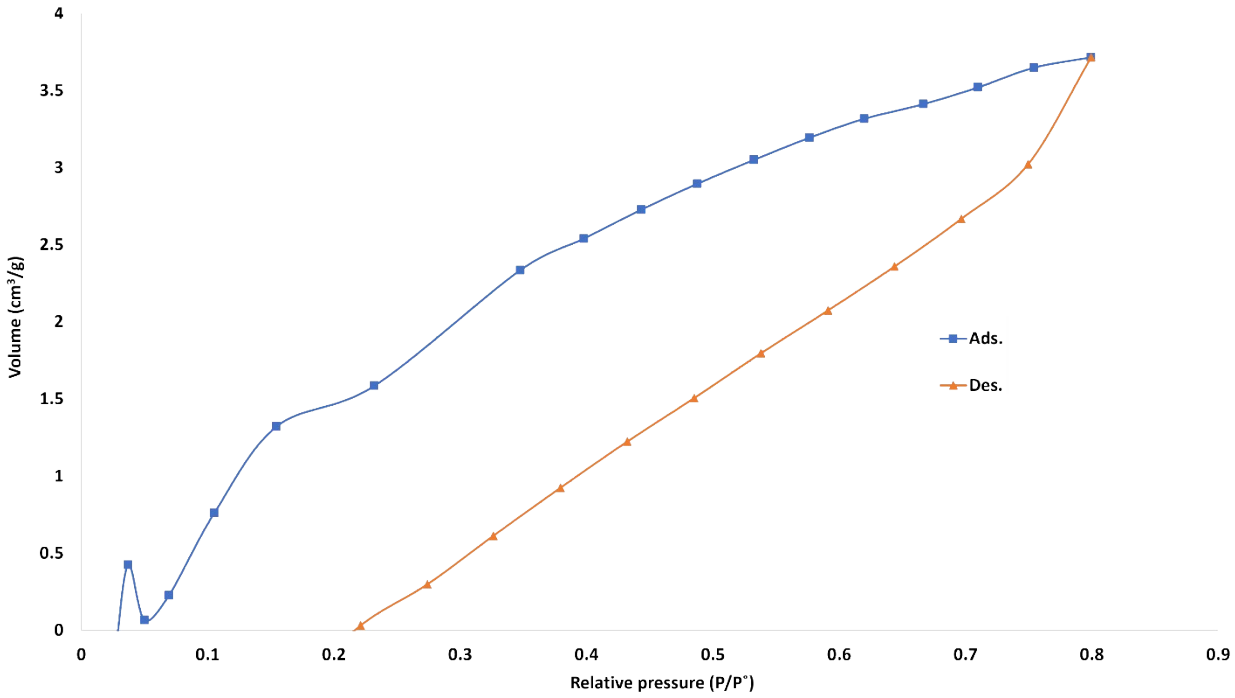

Figure S20. CO_2 adsorption (square)/desorption (triangle) isotherm of **9** at 298 K.

4. References

[1] P. Bhanja, S. Mishra, K. Manna, K. Das Saha, A. Bhaumik, *ACS Omega* **2018**, *3*, 529–535.
[2] P. Puthiaraj, H. S. Kim, K. Yu, W.-S. Ahn, *Microporous Mesoporous Mater.* **2020**, *297*, 110011.
[3] O. M. Yaghi, M. J. Kalmutzki, C. S. Diercks, in *Introd. Reticular Chem.*, John Wiley & Sons, Ltd, **2019**, pp. 197–223.
[4] L. Grunenberg, G. Savasci, M. W. Terban, V. Duppel, I. Moudrakovski, M. Etter, R. E. Dinnebier, C. Ochsenfeld, B. V. Lotsch, *J. Am. Chem. Soc.* **2021**, *143*, 3430–3438.
[5] H. Liu, J. Chu, Z. Yin, X. Cai, L. Zhuang, H. Deng, *Chem* **2018**, *4*, 1696–1709.
[6] D. A. Köse, H. Necefoğlu, *J. Therm. Anal. Calorim.* **2008**, *93*, 509–514.
[7] K. L. Wert, S. Chackalamannil, E. Miller, D. R. Dalton, D. E. Zacharias, J. P. Glusker, *J. Org. Chem.* **1982**, *47*, 5141–5150.
[8] L. Ascherl, T. Sick, J. T. Margraf, S. H. Lapidus, M. Calik, C. Hettstedt, K. Karaghiosoff, M. Döblinger, T. Clark, K. W. Chapman, F. Auras, T. Bein, *Nat. Chem.* **2016**, *8*, 310–316.